Supplementary Information

Olfactory sensory neuron population expansions influence projection neuron adaptation and enhance odour tracking

Suguru Takagi, Gizem Sancer, Liliane Abuin, S. David Stupski, J. Roman Arguello, Lucia L. Prieto-Godino, David L. Stern, Steeve Cruchet, Raquel Álvarez-Ocaña, Carl F. R. Wienecke, Floris van Breugel, James M. Jeanne, Thomas O. Auer and Richard Benton

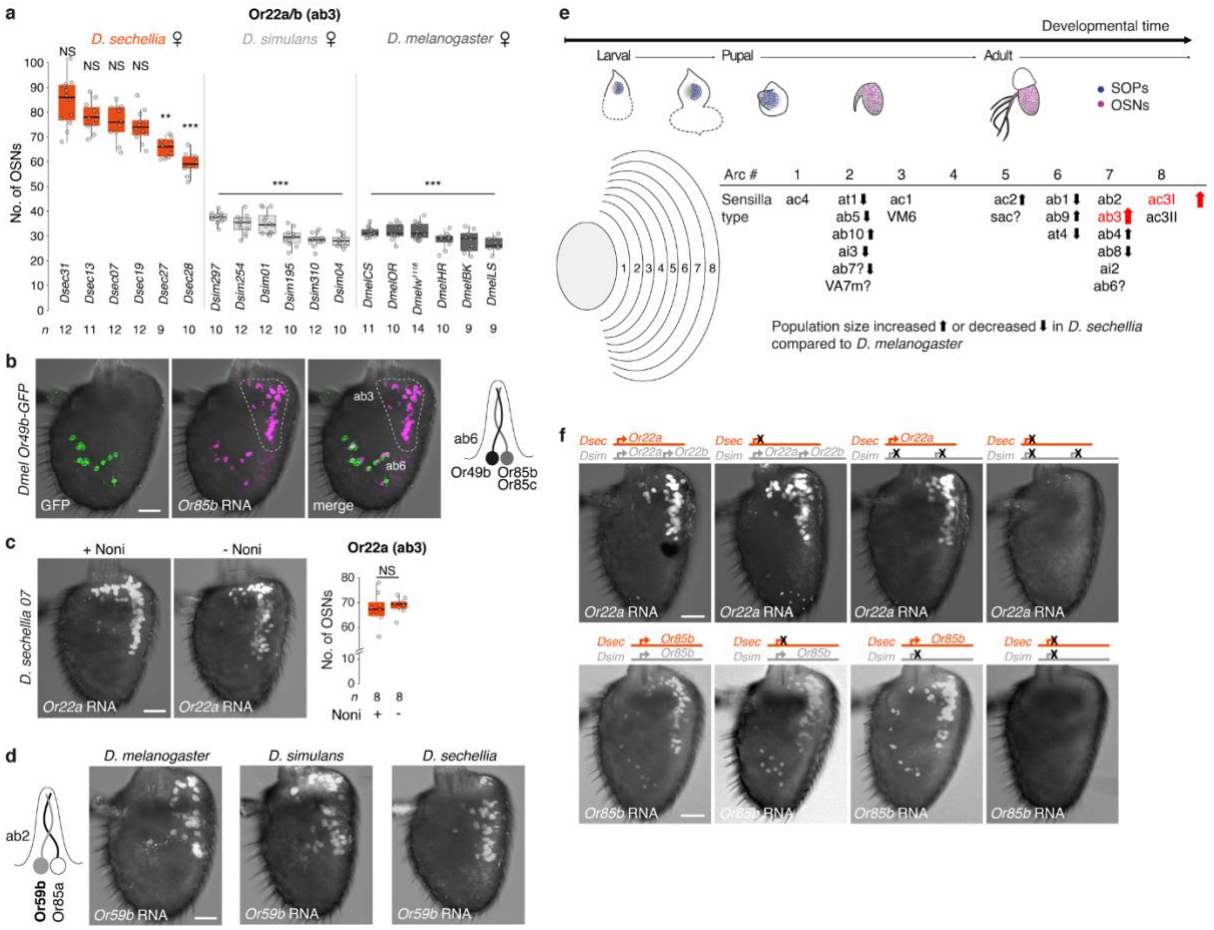

Supplementary Figure 1. Investigation of potential mechanisms underlying the expansion of the ab3 sensillum population in *D. sechellia*.

a, Quantification of *Or22a/(b)* RNA expressing OSNs in the antenna of six *D. sechellia*, *D. simulans* and *D. melanogaster* strains. For strain details see Supplementary Table 1. Comparisons to *Dsec07* (genetic background of transgenic lines) are shown. For these and all other box plots, the centre line represent the median, the box bounds represent the first and third quartiles, and whiskers depict at maximum 1.5× the interquartile range; individual data points are overlaid. Wilcoxon signed-rank test (two-sided), *P* values adjusted for multiple comparisons using the Benjamini and Hochberg method: *** $P < 0.001$; ** $P < 0.01$; NS, not significant ($P > 0.05$).

b, Top, immunofluorescence for GFP and RNA FISH for *Or85b* on whole-mount antennae from *D. melanogaster Or49b-GFP* animals. Or85b neurons are housed in ab3 (paired with Or22a neurons) and ab6 sensilla (paired with Or49b neurons), but only the ab3 population is expanded in *D. sechellia* (Fig. 1c). Scale bar, 25 µm. Here and in subsequent panels and figures, representative images obtained from at least three independent biological replicates are shown.

c, Comparison of the number of *Or22a* RNA-expressing OSNs in the antenna of *D. sechellia* raised on (left) and without (right) noni supplement. Scale bar, 25 µm. Quantification to the right. Wilcoxon signed-rank test (two-sided): NS $P > 0.05$.

d, Left, schematic of the ab2 sensillum housing Or59b and Or85a neurons. Right, RNA FISH for *Or59b* on whole-mount antennae from *D. melanogaster, D. simulans* and *D. sechellia* wild-type animals. Scale bar, 25 µm.

e, Top, schematic of developmental transitions from the larval antennal disc to the

adult antenna. Schematic of the larval antennal disc, within which concentric arcs of sensory organ progenitors (SOPs) are specified, each of which gives rise to a sensillum. Different SOP types have a stereotyped developmental origin in a given arc (adapted from[1]). Arrows indicate the change in relative population size in *D. sechellia* compared to *D. melanogaster*. No obvious relationship between ab3 number increase and compensatory reduction in sensilla derived from SOPs in the same or neighbouring arcs is evident.
f, Representative images of RNA FISH for the reciprocal hemizygosity tests at the *Or22a/b* and *Or85c/b* loci shown in Fig. 1d. Schematics on top illustrate expression from the respective alleles.

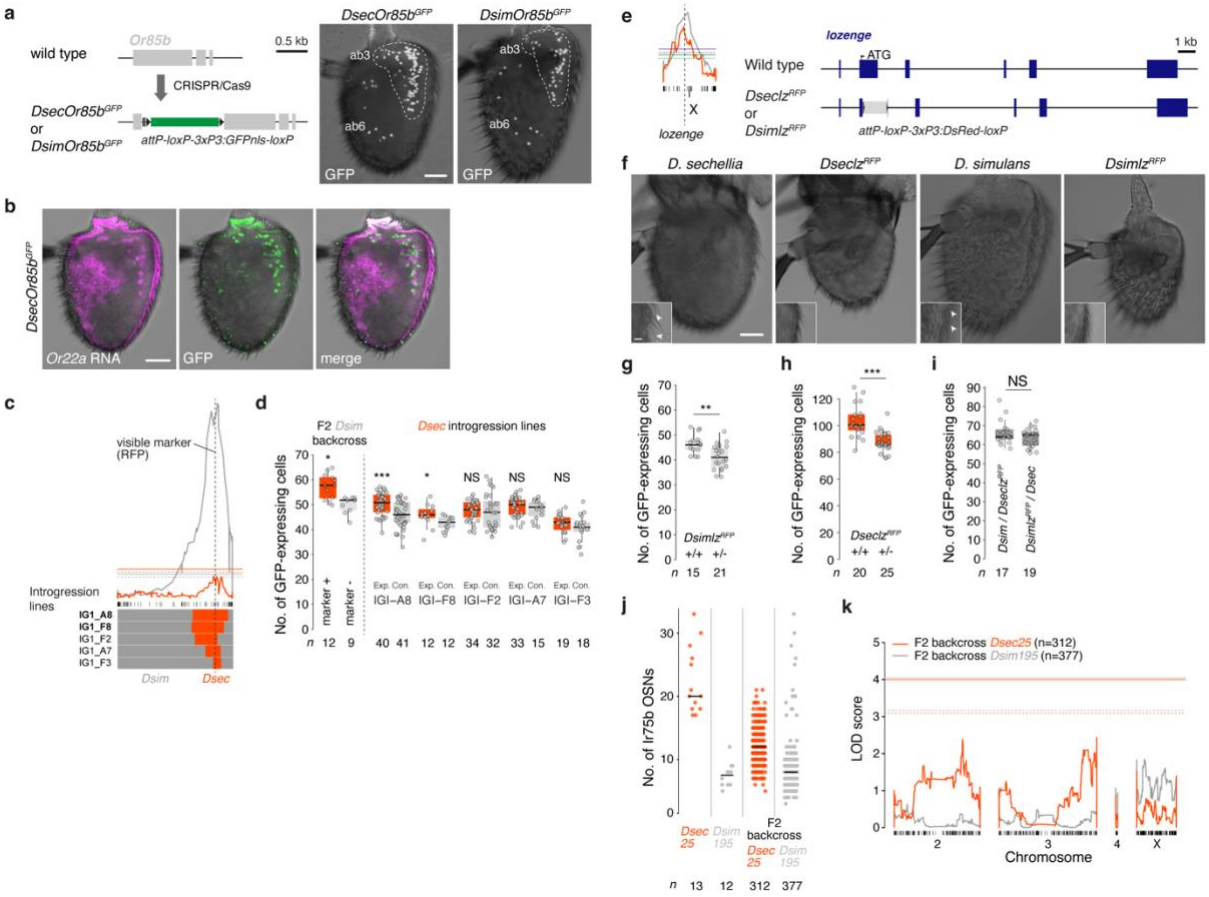

Supplementary Figure 2. Genetic analysis of OSN cell number expansion.
a, Left, schematic depicting the introduction of a nuclear-localised GFP reporter (GFPnls) at the *Or85b* locus of *D. sechellia* and *D. simulans* via CRISPR/Cas9 genome engineering. Right, GFP signal in antennae of *DsecOr85b*^{GFP} and *DsimOr85b*^{GFP} animals. Scale bar, 25 µm.
b, Immunofluorescence for GFP and *Or22a* RNA FISH on whole-mount antennae from *DsecOr85b*^{GFP} animals. Scale bar, 25 µm.
c, Introgression of chromosomal fragments marked with a transgenic RFP marker (dashed line) from *D. sechellia* into *D. simulans* spanning different extents of the QTL peak on chromosome 3.
d, Left, quantification of GFP-expressing neurons in F2 backcrosses of the *D. sechellia* RFP transgenic line to *D. simulans Or85b*^{GFP} flies comparing RFP positive and negative siblings. Right, quantification of GFP-expressing neurons in the five *D. sechellia* introgression lines depicted in c comparing RFP positive and negative siblings. Wilcoxon signed-rank test (two-sided): *** $P < 0.001$; * $P < 0.05$; NS $P > 0.05$.
e, Left, location of the *lozenge* (*lz*) gene (dashed line) relative to the QTL peaks detected on the X chromosome. Right, schematics depicting *lz* organisation and the structure of mutant alleles in both *D. sechellia* and *D. simulans*. The fluorescent marker was integrated into the first coding exon.
f, Comparison of antennal morphology in wild-type and *lz* mutant *D. sechellia* and *D. simulans*. In both species, loss of *lz* results in a lack of basiconic sensilla (white arrowheads) compared to wild-type, similar to *D. melanogaster lz* mutants[2]. Scale bar, 25 µm; inset scale bar, 5 µm.
g, Quantification of GFP-expressing neurons in *DsimlzRFP* heterozygote mutant and wild-type siblings. Wilcoxon signed-rank test (two-sided): ** $P < 0.01$.

h, Quantification of GFP-expressing neurons in *Dseclz*^{RFP} heterozygote mutant and wild-type siblings. Wilcoxon signed-rank test (two-sided): *** $P < 0.001$.
i, Quantification of GFP-expressing neurons in *trans*-heterozygote hybrid siblings carrying either a *Dseclz*^{RFP} or *Dsimlz*^{RFP} allele. Wilcoxon signed-rank test (two-sided): NS $P > 0.05$.
j, Quantification of Ir75b neurons in wild-type *D. sechellia* (DSSC 14021-0248.25) and *D. simulans* (DSSC 14021-0251.195) (mixed genders) and respective F2 progeny derived from backcrosses of F1 hybrid females to either parental strain (mixed genders). The black line indicates the mean cell number.
k, Logarithm of odds (LOD) score across all four chromosomes for loci impacting Ir75b neuron numbers based on phenotyping data shown in **j**. Dashed horizontal lines mark $P = 0.05$; non-dashed horizontal lines mark $P = 0.01$.

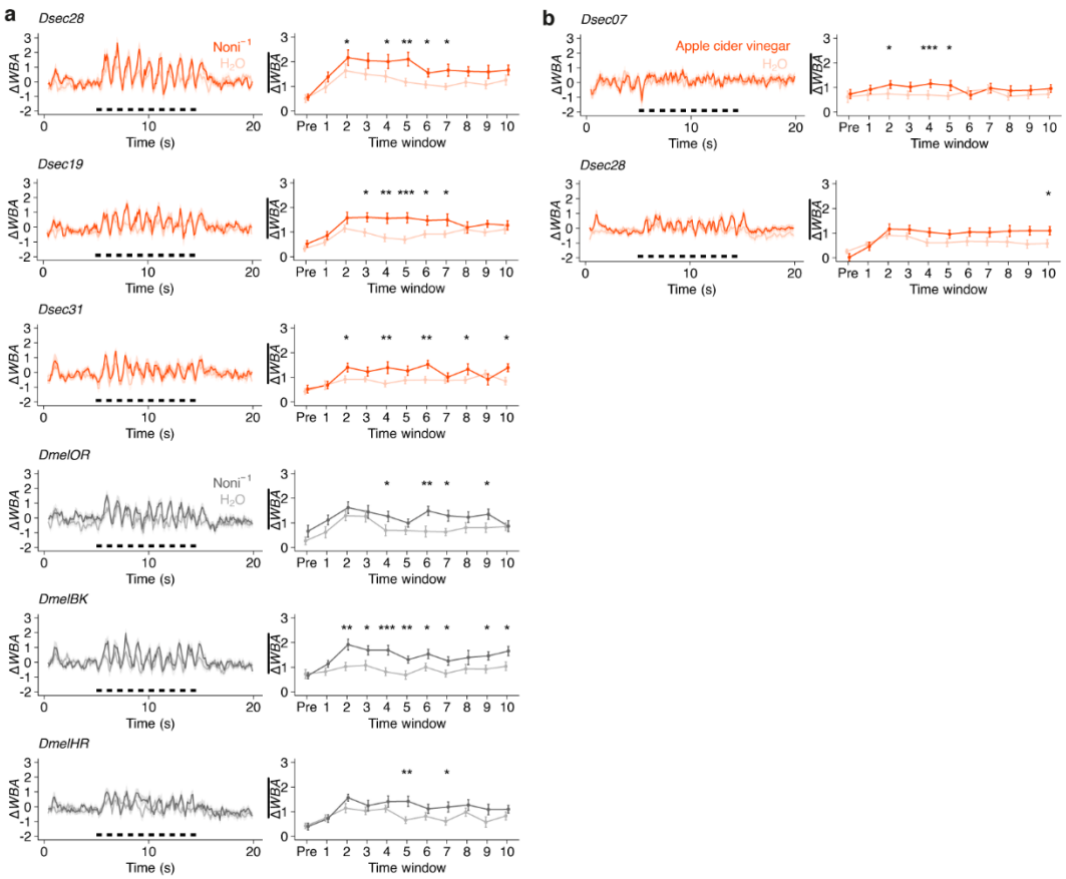

Supplementary Figure 3. Odour-tracking behaviour of wild-type strains.
a, Odour-tracking behaviour towards noni juice in other wild-type strains of *D. sechellia* and *D. melanogaster* (see Supplementary Table 1), plotted as in Fig. 2b. Paired *t*-test (two-sided): *** $P < 0.001$; ** $P < 0.01$; * $P < 0.05$; otherwise $P > 0.05$. $n = 30$ (*DmelBK*, *DmelHR*, *Dsec19*, *Dsec31*) or 27 (*DmelOR*, *Dsec28*) animals.
b, Odour-tracking behaviour towards apple cider vinegar in wild-type *D. sechellia* strains. Paired *t*-test (two-sided): *** $P < 0.001$; * $P < 0.05$; otherwise $P > 0.05$. $n = 30$ animals each.

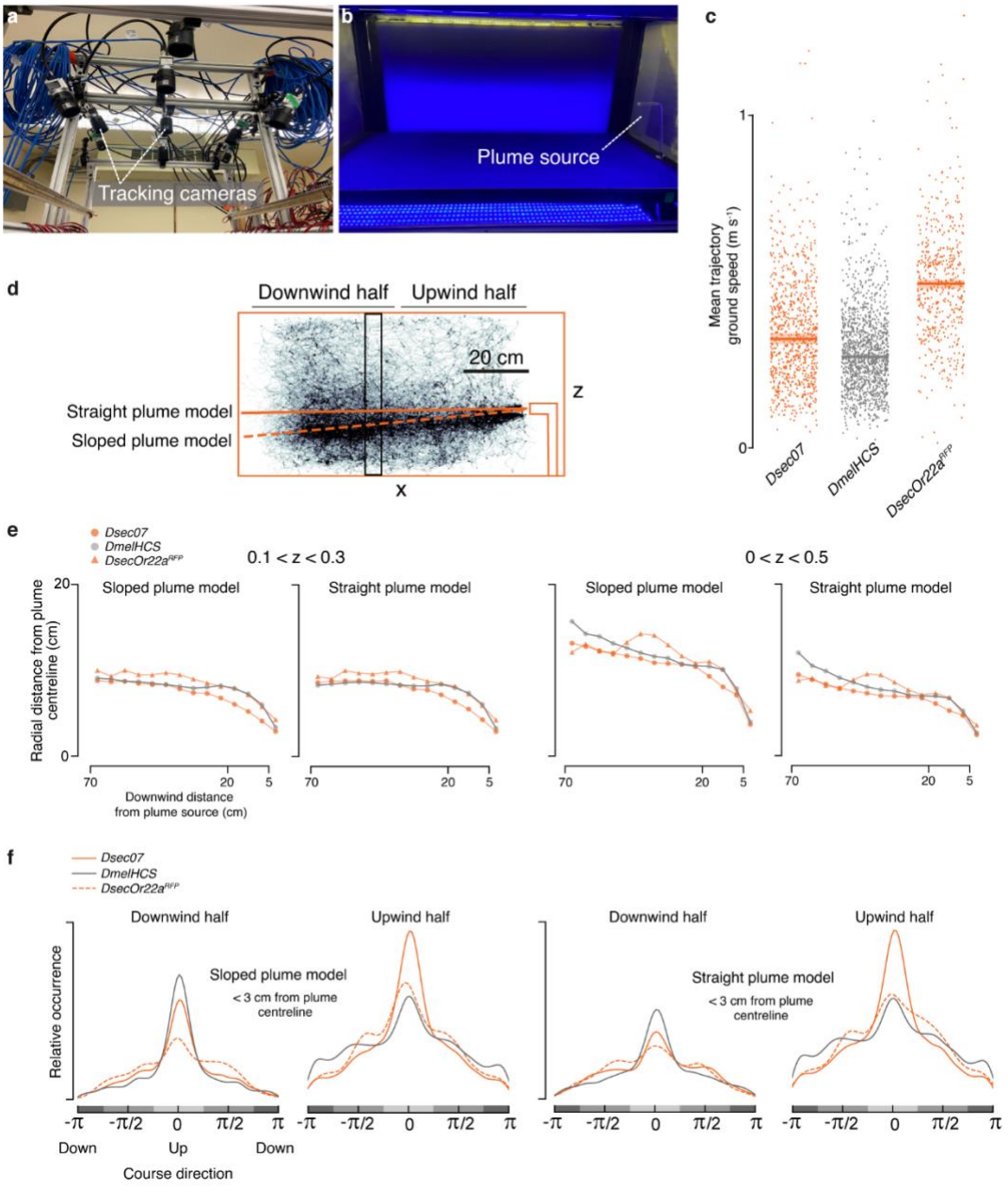

Supplementary Figure 4. Odour tracking in a wind tunnel.

a, Array of 12 tracking cameras above the wind tunnel used for 3D tracking of flies in the presence of a noni plume.

b, Side view of wind tunnel system along with the acrylic port used to flux noni odour into the tunnel volume.

c, Comparison of mean trajectory ground speeds for the three genotypes studied. The higher ground speed of *D. sechellia Or22a* mutants likely reflects, in part, defects in noni odour plume detection of these animals, as studies in *D. melanogaster* demonstrate that odour encounter leads to deceleration of animals during flight[3,4].

d, Schematic of two plume models used to analyse data compared to the point cloud distribution of *D. sechellia* trajectories in the wind tunnel volume: a “straight” model (solid orange line), which is aligned in space with the odour port, and a “sloped” model (dashed orange line), for which the plume sinks by 5 cm from the odour port to the tunnel end.

e, Radial distance calculations comparing mean radial distance of points from the plume centreline considering either the sloped or straight plume model (left two plots). The same data are also shown without the restriction to limit this analysis to 10 cm above or below the plume's altitude (right two plots).
f, Left, course direction distributions within a 3 cm radius of the plume centreline for either the sloped plume model (as in Fig. 2g) for the downwind and upwind halves of the wind tunnel, up to 5 cm downwind from the plume origin. Right, the same analysis assuming a straight plume model.

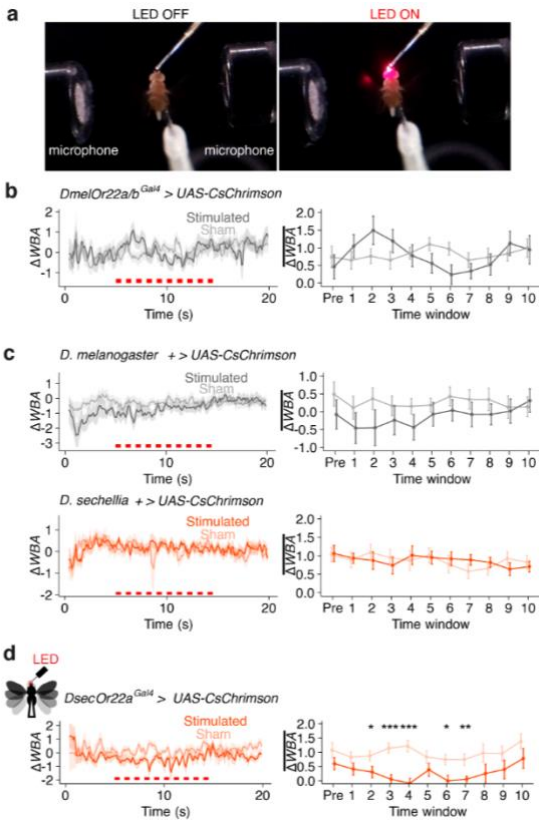

Supplementary Figure 5. Additional conditions of optogenetic stimulation.
a, Optic fibre-mediated illumination of one antenna in the tethered fly. The photo was taken from below the apparatus.
b, Behavioural responses to optogenetic stimulation of Or22a/b OSNs in *D. melanogaster* using a *Gal4* knock-in line (see Fig. 3a for methodological details) Genotype: *D. melanogaster w;Or22a/b^{Gal4}/UAS-CsChrimson-Venus*. Left, time course of *ΔWBA*. Right, quantification within each phase. Paired *t*-test (two-sided): $P > 0.05$.
c, Behavioural responses to optogenetic stimulation of effector control flies (*UAS-CsChrimson-Venus*) in *D. melanogaster* (left) and *D. sechellia* (right). Paired *t*-test (two-sided): $P > 0.05$. Genotypes: *D. melanogaster w;+/UAS-CsChrimson-Venus, D. sechellia w;;+/UAS-CsChrimson-Venus.*
d, Behavioural responses to optogenetic stimulation of Or22a OSNs in the left antenna of *D. sechellia* induces leftward turning behaviour (resulting in reduced *ΔWBA* values compared to control flies). Paired *t*-test (two-sided): ** $P < 0.01$; * $P < 0.05$; otherwise $P > 0.05$. Genotype as in Fig. 3a.

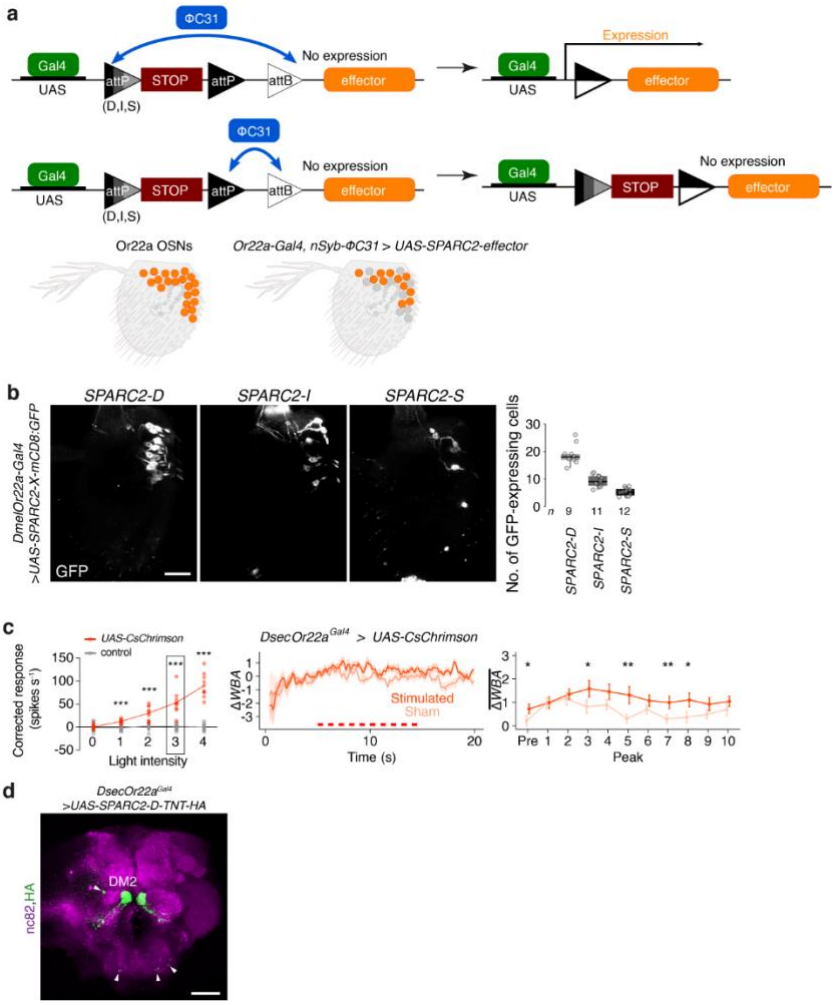

Supplementary Figure 6. SPARC2-based manipulation of a subset of Or22a OSNs.

a, Schematic illustrating the principle of SPARC2[5]. Top, ΦC31-mediated recombination leads to removal of a stop cassette flanked by attP sites. Co-expression of Gal4 in the same cell leads to transcriptional activation of an effector gene. Middle, recombination with an alternative attP site does not lead to a functional read-out. Depending on the attP version present in the cassette, recombination efficiencies vary (D, dense; I, intermediate; S, sparse). Bottom, after recombination, a proportion of Gal4-expressing cells – in this study, Or22a OSNs – will express the respective SPARC2 transgene.

b, Left, immunofluorescence for GFP on whole-mount antennae from *D. melanogaster* expressing different *SPARC2-X-GFP* versions in Or22a neurons. Right, quantification of the number of Or22a OSNs labelled by SPARC2 versions. Genotypes: *D. melanogaster nSyb-ΦC31/+;Or22a^{Gal4}/UAS-SPARC2-X-GFP*. The SPARC2-D transgene labelled ~50% of Or22a OSNs (compare with Fig. 1c) and was therefore used to generate transgenic constructs in *D. sechellia*.

c, Optogenetic stimulation of Or22a OSNs in *D. sechellia* using a lower light intensity. Electrophysiological measurements confirm that this light intensity evokes a similar degree of OSN firing as in the SPARC2-D-CsChrimson experiment. Paired *t*-test (two-sided): * $P < 0.05$; otherwise $P > 0.05$. Electrophysiological data are re-plotted from Fig. 3a.

d, Immunofluorescence for HA and nc82 on a whole-mount brain of *D. sechellia* *Or22a*^{Gal4} transgenic flies expressing *UAS-SPARC2-D-TNT-HA-GeCO*, revealing selective strong expression in Or22a OSNs projecting to DM2. The white arrowheads point to a few cells (putative glia due to their apparent lack of processes) labelled in the central brain. Scale bar, 50 μm.

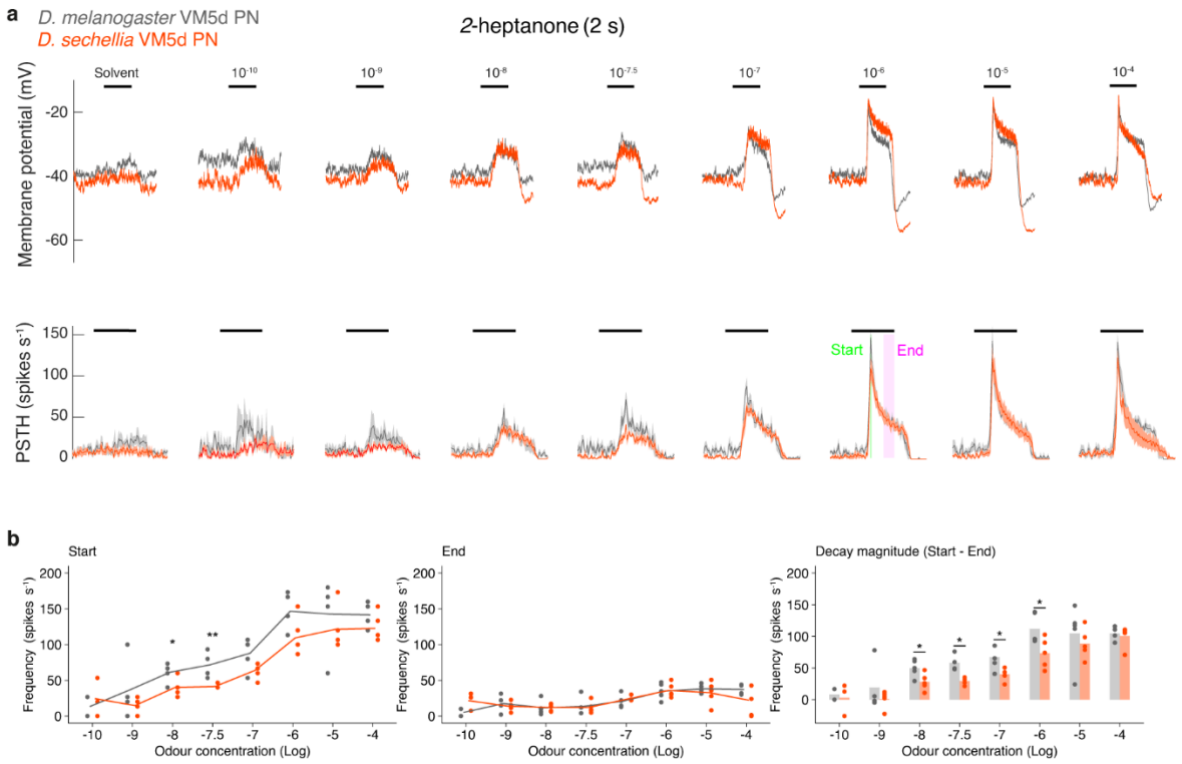

Supplementary Figure 7. Whole-cell patch clamp recordings from VM5d PNs.
a, Voltage traces (top) and peri-stimulus time histograms (PSTH, bottom) of VM5d PN responses to a dilution series of *2*-heptanone. Mean values are shown for the voltage trace and mean ± SEM are shown for the PSTH. *n* = 2-5 animals. Genotypes as in Fig. 4f.
b, Start and end responses of VM5d PNs to a dilution series of *2*-heptanone. Quantification of spike frequencies at the start (first 50 ms), end (last 500 ms before odour offset) and the decay magnitude (start - end) are shown. Student's *t*-test (two-sided): * $P < 0.05$. *n* = 2-5 animals (exact n, mean values and SEM for each concentration are provided in Supplementary Data 1).

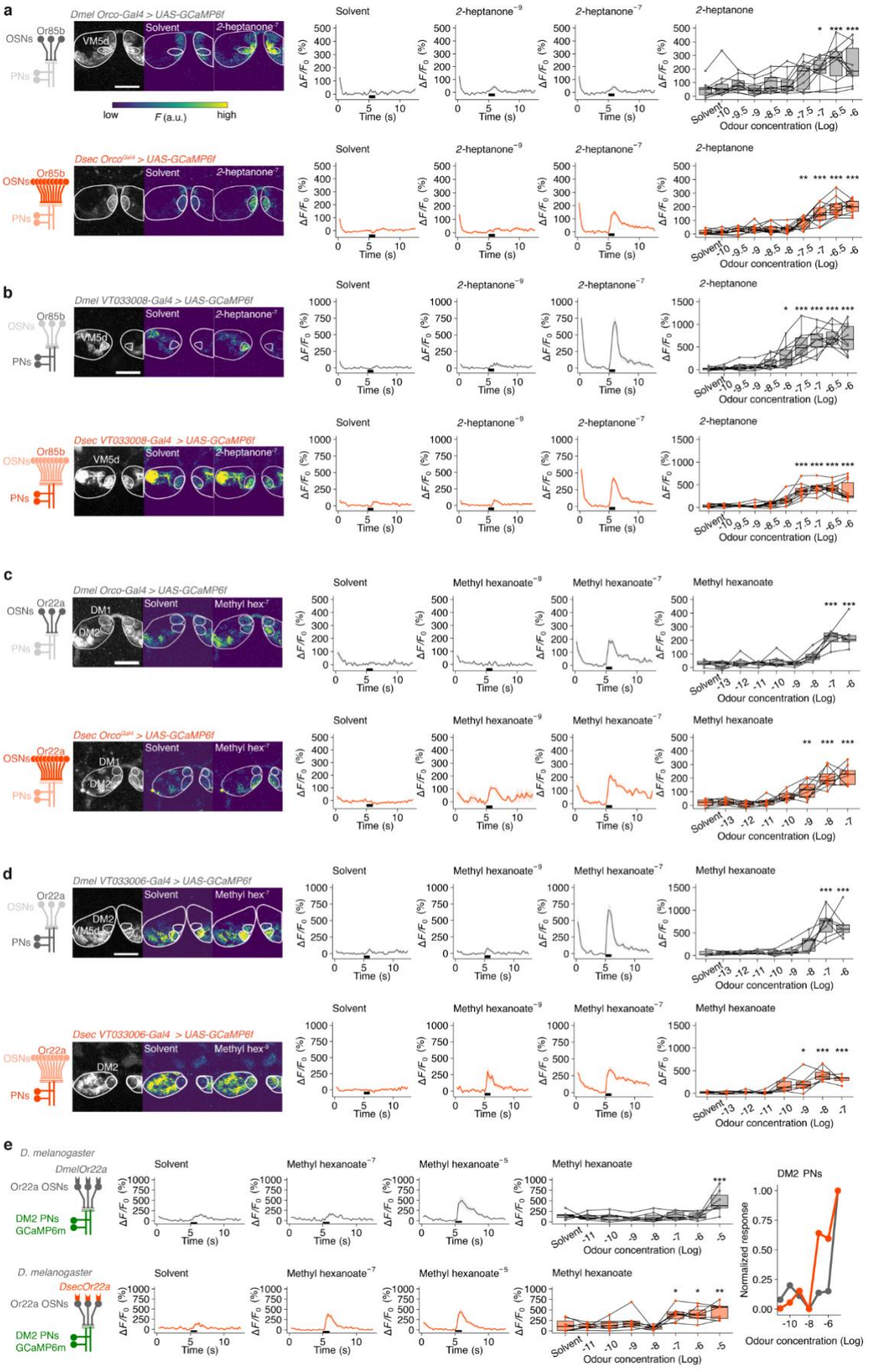
a
Dmel Orco-Gal4 > UAS-GCaMP6f
OSNs
Or85b
PNs
VM5d
Solvent
2-heptanone-7
low
F (a.u.)
high
Dsec Orco Gal4 > UAS-GCaMP6f
Solvent
2-heptanone-9
2-heptanone-7
2-heptanone
ΔF/F0 (%)
Time (s)
Odour concentration (Log)
b
Dmel VT033008-Gal4 > UAS-GCaMP6f
Dsec VT033008-Gal4 > UAS-GCaMP6f
c
Or22a
DM1
DM2
Methyl hex-7
Methyl hexanoate-9
Methyl hexanoate-7
Methyl hexanoate
Dsec Orco Gal4 > UAS-GCaMP6f
d
Dmel VT033006-Gal4 > UAS-GCaMP6f
Dsec VT033006-Gal4 > UAS-GCaMP6f
e
D. melanogaster
DmelOr22a
Or22a OSNs
DM2 PNs
GCaMP6m
Methyl hexanoate-5
DM2 PNs
Normalized response
D. melanogaster
DsecOr22a

Supplementary Figure 8. Dose-dependent odour responses of OSNs and PNs in Or85b and Or22a pathways.

a,**b**, Representative odour-evoked calcium responses in the axon termini of Or85b OSNs (**a**) and dendrites of VM5d PNs (**b**) in *D. melanogaster* and *D. sechellia.* Far left, schematic of the OSN-PN populations under investigation; the population subject to imaging analysis is shown in a darker colour. Left, representative confocal images of the raw fluorescence of GCaMP6f showing the plane used for imaging with glomerular labels; corresponding solvent and odour stimulus-induced fluorescent changes are also shown. Middle, time courses of responses to solvents and two odour dilutions (mean ± SEM $\Delta F/F_0$, bars indicate the timing of stimulus). Right, quantifications of peak $\Delta F/F_0$ for a dilution series of each odour (Dunnett's test (two-sided), control: solvent, *** $P < 0.001$; ** $P < 0.01$; * $P < 0.05$; otherwise $P > 0.05$). $n = 7$ (*D. melanogaster* OSNs), 8 (*D. sechellia* OSNs), 7 (*D. melanogaster* PNs), 6 (*D. sechellia* PNs) animals. Genotypes as in Fig. 5g.

c,**d**, Representative odour-evoked calcium responses in the axon termini of Or22a OSNs (**c**) and DM2 PNs (**d**) in *D. melanogaster* and *D. sechellia. n* = 10 animals each. Genotypes as in Fig. 5g.

e, Calcium imaging of DM2 PNs in *D. melanogaster Or22a* mutants rescued by *DmelOr22a* (top) or *DsecOr22a* (bottom). Left, time courses of odour responses. Middle, quantifications of peak $\Delta F/F_0$. (Dunnett's test (two-sided), control: solvent, *** $P < 0.001$; ** $P < 0.01$; * $P < 0.05$; otherwise $P > 0.05$). $n = 7$ animals each. Right, normalised GCaMP6f fluorescence changes. Genotypes: *D. melanogaster w*;*Or22a/b*^{Gal4}/*Or22a/b*^{Gal4};*UAS-DmelOr22a*,*VT033006-LexA*/*VT033006-LexA,LexAop-GCaMP6m* (*DmelOr22a* rescue), *w*;*Or22a/b*^{Gal4}/*Or22a/b*^{Gal4};*UAS-DsecOr22a*,*VT033006-LexA*/*VT033006-LexA,LexAop-GCaMP6m* (*DsecOr22a* rescue).

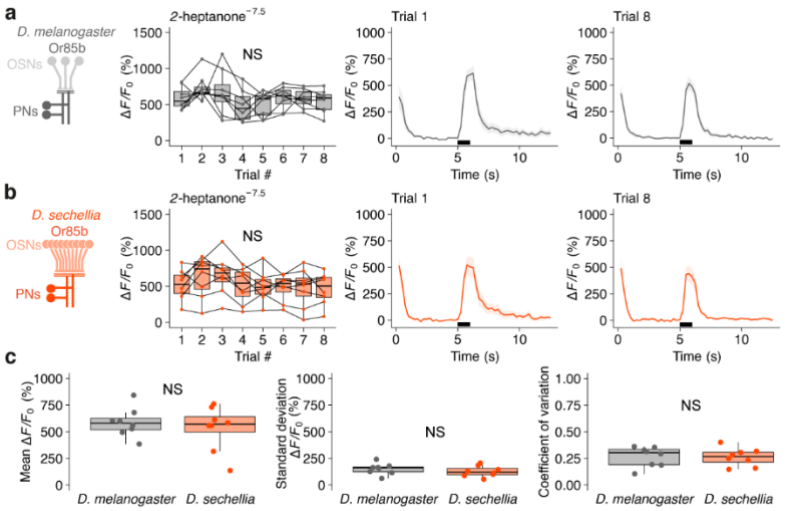

Supplementary Figure 9. Odour response reliability of VM5d PNs.
a,**b**, Calcium responses of VM5d PNs in response to repeated stimulation with *2*-heptanone (concentration (Log) indicated on the figure) in *D. melanogaster* (**a**) and *D. sechellia* (**b**). Left, quantification of peak $\Delta F/F_0$ from eight trials of stimulation. Dunnett's test (two-sided), compared to control (Trial 1): NS $P > 0.05$. $n = 8$ animals each. Right, time courses of responses in trial 1 and 8 shown as mean ± SEM $\Delta F/F_0$. The odour stimulus (1 s) is shown with a black bar. Genotypes as in Fig. 5g.
c, Quantification of mean, standard deviation and coefficient of variation of peak $\Delta F/F_0$ across the eight stimulation trials. Welch's *t*-test: NS $P > 0.05$.

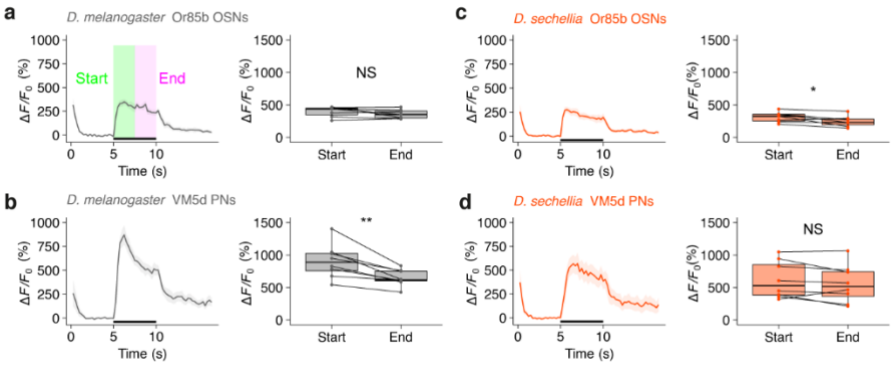

Supplementary Figure 10. *D. sechellia* VM5d PNs exhibit persistent responses to long odour stimulation.

a-**d**, Calcium responses to long odour stimulation of *D. melanogaster* Or85b OSNs (**a**), *D. melanogaster* VM5d PNs (**b**), *D. sechellia* Or85b OSNs (**c**), and *D. sechellia* VM5d PNs (**d**). Left, time courses of the odour response (mean ± SEM $\Delta F/F_0$). Bars indicate the timing of stimulation (5 s). Right, maximum $\Delta F/F_0$ in the first and last 2.5 s time windows are compared. Paired *t*-test (two-sided): ** $P < 0.01$; * $P < 0.05$; NS $P > 0.05$. $n = 7$ (OSNs) or 8 (PNs) animals for both species. Genotypes as in Fig. 5g.

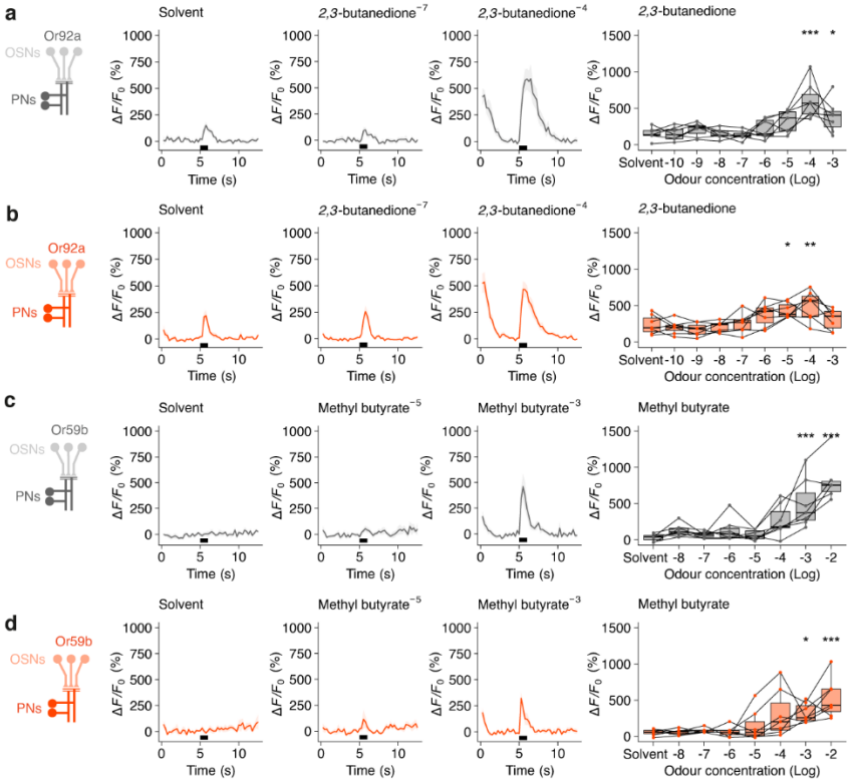

Supplementary Figure 11. Odour response sensitivity in control glomeruli.
a-**d**, Odour-evoked dose-dependent calcium responses in control glomeruli of *D. melanogaster* VA2 (Or92a) PNs (**a**), *D. sechellia* VA2 PNs (**b**), *D. melanogaster* DM4 (Or59b) PNs (**c**), and *D. sechellia* DM4 PNs (**d**). Left, time courses in response to solvents and specific odour dilutions (mean ± SEM $\Delta F/F_0$, bars indicate the timing of stimuli). Right, quantifications of peak $\Delta F/F_0$ (Dunnett's test (two-sided), control: solvent, *** $P < 0.001$; ** $P < 0.01$; * $P < 0.05$; otherwise $P > 0.05$). $n = 7$ each. Genotypes as in Fig. 5g.

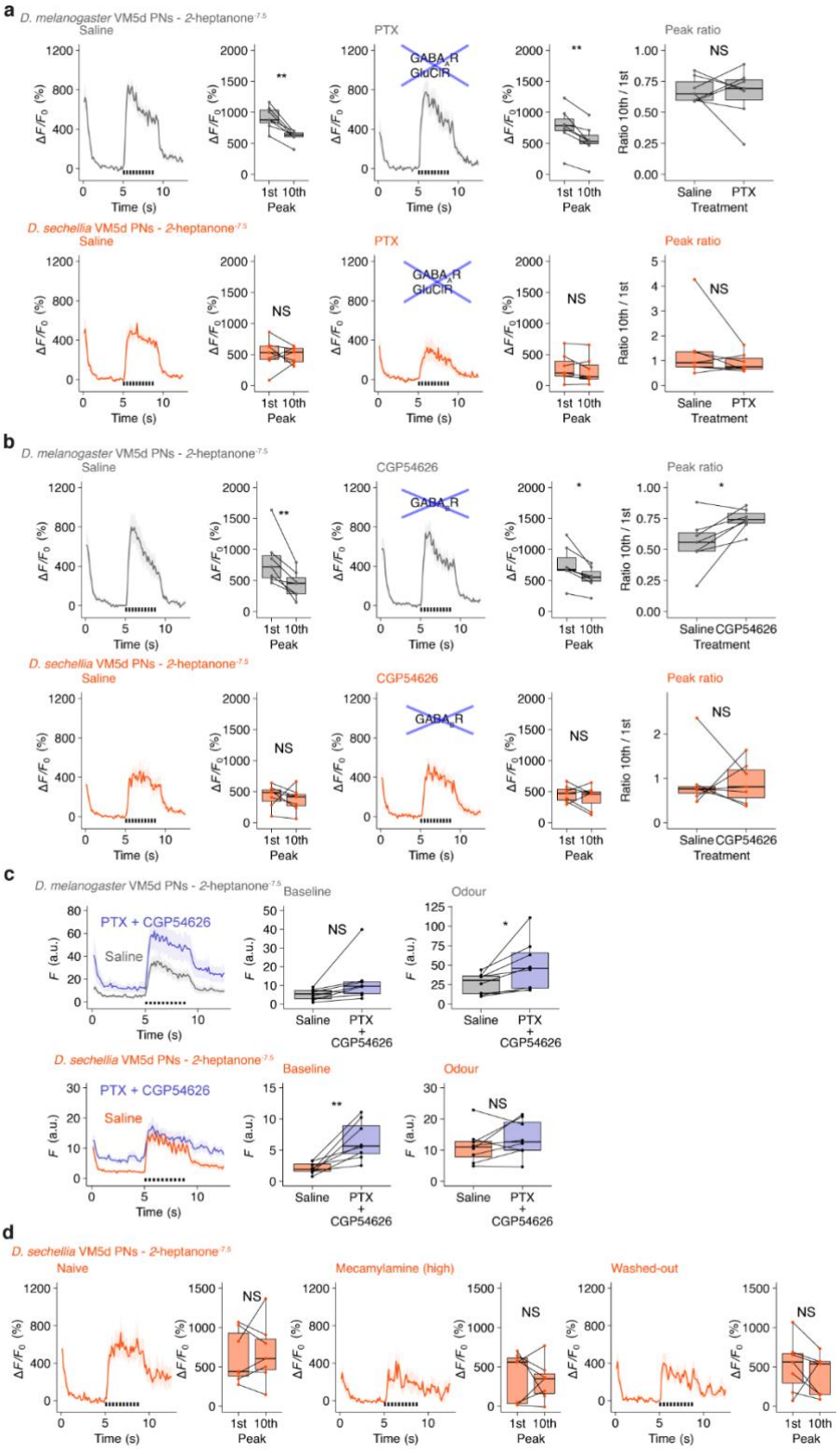

Supplementary Figure 12. Pharmacological manipulations of lateral inhibition. **a**,**b**, Odour pulse responses of VM5d PNs following application of a $GABA_A$ (**a**, Picrotoxin) or $GABA_B$ (**b**, CGP54626) receptor antagonist. PN responses in normal AHL saline (left) or containing 100 µM picrotoxin or 50 µM CGP54626 (middle). The ratio between 10th and 1st odour pulses are shown on the far right. Paired *t*-test (two-

sided): ** $P < 0.01$; * $P < 0.05$; NS $P > 0.05$. $n = 7$ animals each. Genotypes as in Fig. 5g.
c, Raw GCaMP fluorescence intensity in VM5d PNs in *D. melanogaster* (top) and *D. sechellia* (bottom) following GABA antagonist application. Mean fluorescence before (4-5 s; "Baseline") and during (5-9 s; “Odour”) the stimulus was quantified. Paired *t*-test (two-sided): ** $P < 0.01$, * $P < 0.05$, NS $P > 0.05$. $n = 8$ animals each.
d, Odour pulse responses of VM5d PNs following application of a high dose (2 mM) of mecamylamine (nAChR antagonist) to strongly block cholinergic inputs. *D. sechellia* PN responses in normal AHL saline, mecamylamine and AHL saline wash-out are shown. Paired *t*-test (two-sided): NS $P > 0.05$. $n = 7$ animals.

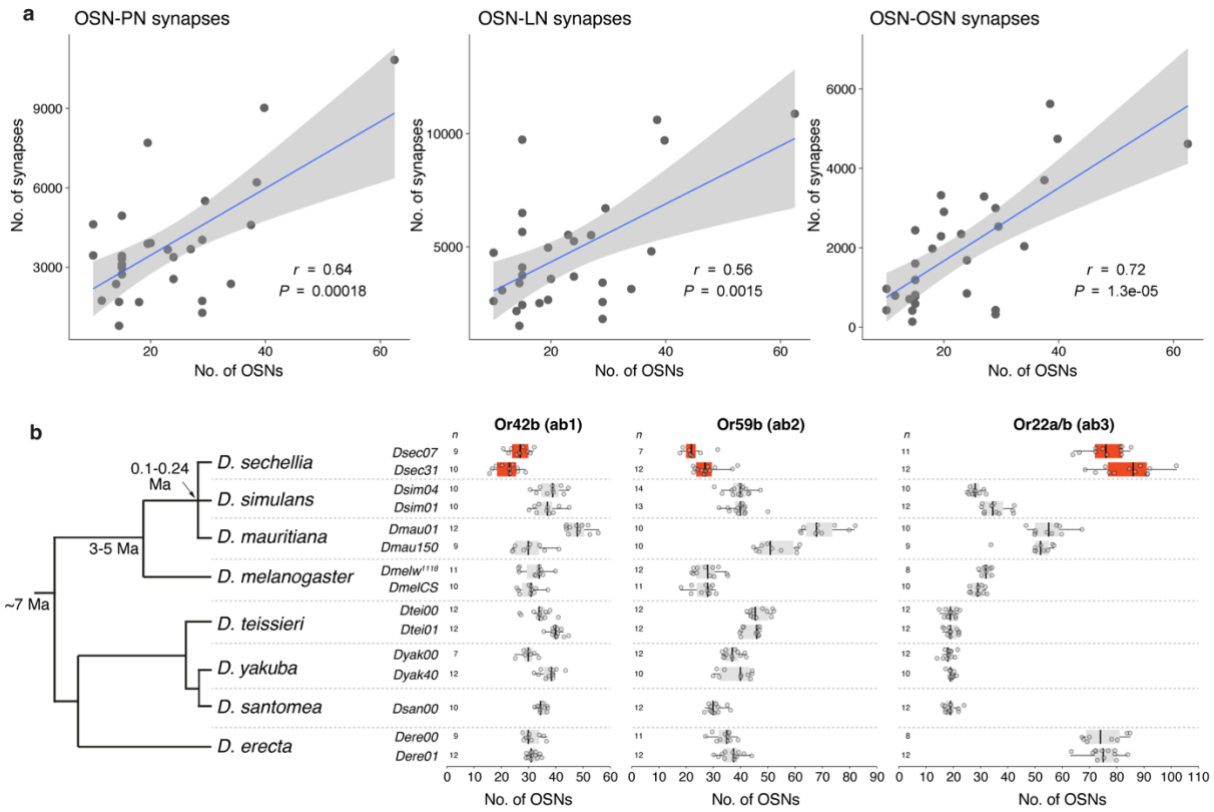

Supplementary Figure 13. Variation in neuron numbers within and across species.

a, Correlation between OSN and synapse numbers across glomeruli, from *D. melanogaster* OSN quantifications[6] and electron microscopic connectome[7] datasets. OSN outputs were quantified separately for connections to PNs (left), LNs (middle) and OSNs (right). *r* and *P* values are calculated by Pearson's correlation analysis.

b, Variation in basiconic sensilla neuron numbers in the *D. melanogaster* species subgroup. Numbers of Or42b, Or59b and Or22a/(b) neurons (housed in ab1, ab2 and ab3 sensilla, respectively) based on RNA FISH on whole-mount antennae of the indicated species/strains. Ma, million years ago. For strain details see Supplementary Table 1.

Supplementary Table 1. Wild-type and transgenic drosophilid lines.

Stock name	Donor plasmid	Parental strain	Species	Method or Reference	Figure
Dsec07		*Drosophila* Species Stock Center [DSSC] 14021-0248.07	*D. sechellia*		Fig. 1, Fig. 2, Sup. Fig. 1, Sup. Fig. 2, Sup. Fig. 3, Sup. Fig. 4, Sup. Fig. 13
Dsec31		DSSC 14021-0248.31	*D. sechellia*		Sup. Fig. 1, Sup. Fig. 3, Sup. Fig. 13
Dsec19		DSSC 14021-0248.19	*D. sechellia*		Sup. Fig. 1, Sup. Fig. 3
Dsec13		DSSC 14021-0248.13	*D. sechellia*		Sup. Fig. 1
Dsec27		DSSC 14021-0248.27	*D. sechellia*		Sup. Fig. 1
Dsec28		DSSC 14021-0248.28	*D. sechellia*		Sup. Fig. 1, Sup. Fig. 3
Dsec25		DSSC 14021-0248.25	*D. sechellia*		Sup. Fig. 2
Dsim297		DSSC 14021-0251.297	*D. simulans*		Sup. Fig. 1
Dsim254		DSSC 14021-0251.254	*D. simulans*		Sup. Fig. 1
Dsim01		DSSC 14021-0251.001	*D. simulans*		Sup. Fig. 1, Sup. Fig. 13
Dsim195		DSSC 14021-0251.195	*D. simulans*		Sup. Fig. 1 Sup. Fig. 2
Dsim310		DSSC 14021-0251.310	*D. simulans*		Sup. Fig. 1
Dsim04		DSSC 14021-0251.004	*D. simulans*		Fig. 1, Sup. Fig. 1, Sup. Fig. 2, Sup. Fig. 13
Dsim03		DSSC 14021-0251.003	*D. simulans*		Sup. Fig. 2
DmelCS		*D. melanogaster Canton-S*	*D. melanogaster*		Fig. 1, Fig. 2, Sup. Fig. 1, Sup. Fig. 13
DmelOR		*Dmel Oregon-R*	*D. melanogaster*		Sup. Fig. 1, Sup. Fig. 3
Dmelw^{1118}		*Dmel w^{1118}*	*D. melanogaster*		Sup. Fig. 1, Sup. Fig. 13
DmelHR		*Dmel Hikone-R*	*D. melanogaster*		Sup. Fig. 1, Sup. Fig. 3
DmelBK		*Dmel Berlin-K*	*D. melanogaster*		Sup. Fig. 1, Sup. Fig. 3
DmelLS		*Dmel Lausanne-S*	*D. melanogaster*		Sup. Fig. 1
DmelHCS		*Dmel Heisenberg CS*	*D. melanogaster*		Figure 2, Sup. Fig. 4
Dmau01		DSSC 14021-0241.01	*D. mauritiana*		Sup. Fig. 13
Dmau150		DSSC 14021-0241.150	*D. mauritiana*		Sup. Fig. 13
Dtei00		DSSC 14021-0257.00	*D. teissieri*		Sup. Fig. 13
Dtei01		DSSC 14021-0257.01	*D. teissieri*		Sup. Fig. 13
Dyak00		DSSC 14021-0261.00	*D. yakuba*		Sup. Fig. 13
Dyak40		DSSC 14021-0261.40	*D. yakuba*		Sup. Fig. 13
Dsan00		DSSC 14021-0271.00	*D. santomea*		Sup. Fig. 13

Dere00		DSSC 14021-0224.00	*D. erecta*		Sup. Fig. 13
Dere01		DSSC 14021-0224.01	*D. erecta*		Sup. Fig. 13
DsecOr22a^{RFP}			*D. sechellia*	[8]	Fig. 1, Fig. 2, Sup. Fig. 1, Sup. Fig. 4
DsecOr85c/b^{RFP}			*D. sechellia*	[8]	Fig. 2
DsecIr75b^{RFP}			*D. sechellia*	[8]	Fig. 2
DsecOr35a^{RFP}			*D. sechellia*	[8]	Fig. 2
DsimOr85b^{GFP}	*DsimOr85b,3xP3-Stinger*	DSSC 14021-0251.003	*D. simulans*	CRISPR knock-in, this study	Sup. Fig. 2
DsimOr85b^{GFP}	*DsimOr85b,3xP3-Stinger*	DSSC 14021-0251.004	*D. simulans*	CRISPR knock-in, this study	Fig. 1, Sup. Fig. 1, Sup. Fig. 2
DsecOr85b^{GFP}	*DsecOr85b,3xP3-Stinger,*	DSSC 14021-0248.07	*D. sechellia*	[8]	Fig. 1, Sup. Fig. 1, Sup. Fig. 2
Dsec pBAC(UAS-CsChrimson-Venus)	*pBAC(UAS-CsChrimson-Venus-3xP3-DsRed)*		*D. sechellia*	*pBAC* integration, this study	Fig. 3, Sup. Fig. 2, Sup. Fig. 5
Dseclz^{RFP}	*pHD-3xP3-DsRed-Dseclz*	*Dsecnanos-Cas9*	*D. sechellia*	CRISPR knock-in, this study	Sup. Fig. 2
Dsimlz^{RFP}	*pHD-3xP3-DsRed-Dsimlz*	DSSC 14021-0251.004	*D. simulans*	CRISPR knock-in, this study	Sup. Fig. 2
DsimOr22a/b^{RFP}			*D. simulans*	[8]	Fig. 1, Sup. Fig. 1
Dmel Or49b-GFP		Bloomington *Drosophila* Stock Center [BDSC]_52653	*D. melanogaster*	[9]	Sup. Fig. 1
Dsec UAS-GCaMP6f			*D. sechellia*	[8]	Fig. 4, Fig. 5, Fig. 6, Sup. Fig. 8, Sup. Fig. 9, Sup. Fig. 10, Sup. Fig. 11, Sup. Fig. 12
Dsec VT033006-Gal4	*VT033006-Gal4* (from[10])	*Dsecwhite*[8]	*D. sechellia*	attB/P integration, this study	Fig. 4, Fig. 5, Fig. 6, Sup. Fig. 8, Sup. Fig. 9, Sup. Fig. 10, Sup. Fig. 11, Sup. Fig. 12
Dsec VT033008-Gal4	*VT033008-Gal4* (from[10])	*Dsecwhite*[8]	*D. sechellia*	attB/P integration, this study	Fig. 4
Dsec UAS-C3PA-GFP			*D. sechellia*	[8]	Fig. 4
Dsec UAS-Dα7-GFP	*p(UAS-Dα7-GFP)* (gift from S. Sigrist[11])	DSSC 14021-0248.30	*D. sechellia*	P-element transgenesis, this study	Fig. 4
Dmel VT033006-Gal4		*Vienna Drosophila Resource Center* [VDRC] ID 202281	*D. melanogaster*	[10]	Fig. 4, Fig. 5, Fig. 6,

					Sup. Fig. 8, Sup. Fig. 9, Sup. Fig. 11, Sup. Fig. 12
Dmel VT033008-Gal4		VDRC_ID 200242	*D. melanogaster*	[10]	Fig. 4
Dmel UAS-C3PA-GFP			*D. melanogaster*	[12]	Fig. 4
Dmel UAS-Dα7-GFP			*D. melanogaster*	[11]	Fig. 4
Dsec VM5d-Gal4	*GMR_86C10-GAL4*[13]	*Dsec-attP40* (T.O.A. *unpublished*)	*D. sechellia*	attB/P integration	Fig. 4, Fig. 5, Sup. Fig. 7
Dsec UAS-myrGFP	*pUAS-myrGFP, QUAS-mtdTomato(3xHA)*[14]	*Dsec-attP40* (T.O.A. *unpublished*)	*D. sechellia*	attB/P integration	Fig. 4, Fig. 5, Sup. Fig. 7
Dmel VM5d-Gal4		BDSC_46820	*D. melanogaster*		Fig. 4, Fig. 5, Sup. Fig. 7
Dmel UAS-GFP		BDSC_52262	*D. melanogaster*		Fig. 4, Fig. 5, Sup. Fig. 7
Dmel UAS-DsecOr22a			*D. melanogaster*	[8]	Sup. Fig. 8
Dmel UAS-DmelOr22a			*D. melanogaster*	[8]	Sup. Fig. 8
Dmel VT33006-LexA	*p(VT033006-LexA)*	*D. melanogaster* attP2	*D. melanogaster*	attB/P integration, this study	Sup. Fig. 8
Dmel LexAop-GCaMP6m		BCSC_44588	*D. melanogaster*	[15]	Sup. Fig. 8
Dmel Orco-Gal4		BDSC_26818	*D. melanogaster*	[16]	Fig. 5, Sup. Fig. 8, Sup. Fig. 10
Dmel UAS-GCaMP6f		BDSC_42747	*D. melanogaster*	[15]	Fig. 5, Fig. 6, Sup. Fig. 8, Sup. Fig. 9, Sup. Fig. 10, Sup. Fig. 11, Sup. Fig. 12
DsecOrco^{Gal4}			*D. sechellia*	[8]	Fig. 5, Sup. Fig. 5, Sup. Fig. 8, Sup. Fig. 10
DsecOr22a^{Gal4}			*D. sechellia*	[8]	Fig. 3, Sup. Fig. 5, Sup. Fig. 6,
Dsec nSyb-ΦC31	*nSyb-ΦC31* (Addgene #133868)	*Dsec-attP26* (T.O.A. *unpublished*)	*D. sechellia*	attB/P integration, this study	Fig. 3, Sup. Fig. 6
Dsec UAS-SPARC2-D-CsChrimson-Venus	*PHD-Dsec-attP40-SPARC2-D-CsChrimson-Venus*	*D. sechellia* nanos-Cas9	*D. sechellia*	CRISPR knock-in, this study	Fig. 3
Dsec UAS-SPARC2-D-TNT-HA	*pHD-Dsec-attP40-SPARC2-D-TNT-HA*	*D. sechellia* nanos-Cas9	*D. sechellia*	CRISPR knock-in, this study	Fig. 3, Sup. Fig. 6
DmelOr22a/b^{Gal4}			*D. melanogaster*	[17]	Sup. Fig. 5
Dmel UAS-CsChrimson-Venus		BDSC_55136	*D. melanogaster*		Fig. 3, Sup. Fig. 5
Dmel Or22a-Gal4		BDSC_9952	*D. melanogaster*		Fig. 3, Sup. Fig. 6
Dmel nSyb-ΦC31		BDSC_84151	*D. melanogaster*		Sup. Fig. 6

Dmel UAS-SPARC2-S-GFP		BDSC_84148	*D. melanogaster*		Sup. Fig. 6
Dmel UAS-SPARC2-I-GFP		BDSC_84147	*D. melanogaster*		Sup. Fig. 6
Dmel UAS-SPARC2-D-GFP		BDSC_84146	*D. melanogaster*		Sup. Fig. 6

Supplementary Table 2. Oligonucleotides used to generate single sgRNA expression vectors, *in situ* probe templates and *pBac* transgenesis vectors. Overhangs used for Gibson Assembly are shown in lowercase.

Target	Forward primer (5'-3')	Reverse primer (5'-3')
DsimOr85b sgRNA	GTCGCAAATAATCCAACGAAGCCC	AAACGGGCTTCGTTGGATTATTTG
DsecOr47a in situ probe	ATGAAGCCAACGGAAATCCAAAAACCC	TTTCTGCACAAACCATTAAGAAGCTGC
DsecOr88a in situ probe	ATGGAAAGTTTCCTCCAAGTACAG	GATGAGAAGGCCTCCATGTTTG
pUAS-ChR2 CsChrimson	atgccataggccacctattcgtcttcctacTGGGCGCGCCTAGTATGTAT	ccgagtctctgcactgaacattgtcagatcGGCCAGATCGATCCAGACAT
pUC57(3xP3-DsRed)	cataggccacctattcgtcttcctactgggATTACGCCAAGCTTGCATGC	tcagcgccctgcaccattatgttccggaggCCAGTGAATTCGAGCTCGGT

Supplementary Table 3. Oligonucleotides used to generate multi-sgRNA expression vectors.

Target	Name	Sequence (5'-3')	Resulting sgRNAs
Dseclz & Dsimlz	*PCR1fwd*	GCGGCCCGGGTTCGATTCCCGGCCGATGCAGAGGCGTCTGCTCTGCCGCCGTTTTAGAGCTAGAAATAGCAAG	sgRNA1: GAGGCGTCTGCTCTGCCGCC
	PCR1rev	ATCGCTCCATCCACAATAGATGCACCAGCCGGGAATCGAACCC	sgRNA2: TCTATTGTGGATGGAGCGAT
	PCR2fwd	TCTATTGTGGATGGAGCGATGTTTTAGAGCTAGAAATAGCAAG	sgRNA3: TAATAACAACGCCGTTCACC
	PCR2rev	ATTTTAACTTGCTATTTCTAGCTCTAAAACGGTGAACGGCGTTGTTATTATGCACCAGCCGGGAATCGAACCC	

Supplementary References

1. Chai PC, Cruchet S, Wigger L, Benton R. Sensory neuron lineage mapping and manipulation in the *Drosophila* olfactory system. *Nat Commun.* **10**, 643 (2019).

2. Gupta BP, Flores GV, Banerjee U, Rodrigues V. Patterning an epidermal field: *Drosophila* lozenge, a member of the AML-1/Runt family of transcription factors, specifies olfactory sense organ type in a dose-dependent manner. *Dev. Biol.* **203**, 400-411 (1998).

3. Saxena N, Natesan D, Sane SP. Odor source localization in complex visual environments by fruit flies. *J Exp Biol.* **221**, jeb172023 (2018).

4. Stupski SD, van Breugel F. Wind Gates Search States in Free Flight. *bioRxiv.* doi:10.1101/2023.1111.1130.569086 (2024).

5. Isaacman-Beck J*, et al.* SPARC enables genetic manipulation of precise proportions of cells. *Nat. Neurosci.* **23**, 1168-1175 (2020).

6. Grabe V, Baschwitz A, Dweck HKM, Lavista-Llanos S, Hansson BS, Sachse S. Elucidating the Neuronal Architecture of Olfactory Glomeruli in the *Drosophila* Antennal Lobe. *Cell Rep.* **16**, 3401-3413 (2016).

7. Schlegel P*, et al.* Information flow, cell types and stereotypy in a full olfactory connectome. *Elife.* **10**, e66018 (2021).

8. Auer TO*, et al.* Olfactory receptor and circuit evolution promote host specialization. *Nature.* **579**, 402-408 (2020).

9. Couto A, Alenius M, Dickson BJ. Molecular, anatomical, and functional organization of the *Drosophila* olfactory system. *Curr Biol.* **15**, 1535-1547 (2005).

10. Tirian L, Dickson BJ. The VT GAL4, LexA, and split-GAL4 driver line collections for targeted expression in the *Drosophila* nervous system. *bioRxiv.* doi:10.1101/198648 (2017).

11. Leiss F*, et al.* Characterization of dendritic spines in the *Drosophila* central nervous system. *Dev Neurobiol.* **69**, 221-234 (2009).

12. Ellis KE*, et al.* Evolution of connectivity architecture in the *Drosophila* mushroom body. *Nat Commun.* **15**, 4872 (2024).

13. Jenett A*, et al.* A GAL4-driver line resource for *Drosophila* neurobiology. *Cell Rep.* **2**, 991-1001 (2012).

14. Talay M*, et al.* Transsynaptic Mapping of Second-Order Taste Neurons in Flies by *trans*-Tango. *Neuron.* **96**, 783-795 e784 (2017).

15. Chen TW*, et al.* Ultrasensitive fluorescent proteins for imaging neuronal activity. *Nature.* **499**, 295-300 (2013).

16. Wang JW, Wong AM, Flores J, Vosshall LB, Axel R. Two-photon calcium imaging reveals an odor-evoked map of activity in the fly brain. *Cell.* **112**, 271-282 (2003).

17. Chahda JS, Soni N, Sun JS, Ebrahim SAM, Weiss BL, Carlson JR. The molecular and cellular basis of olfactory response to tsetse fly attractants. *PLOS Genet.* **15**, e1008005 (2019).